Huyen, PT.; Nam, LTH.; Vinh, TQ.; Martínez, C.; Parvulescu, VI. (2018). ZSM-5/SBA-15 versus Al-SBA-15 as supports for the hydrocracking/hydroisomerization of alkanes. Catalysis Today. 306:121-127. https://doi.org/10.1016/j.cattod.2017.03.040

ZSM-5/SBA-15 versus Al-SBA-15 as supports for the hydrocracking/ hydroisomerization of alkanes

Pham T. Huyen[1]*, Le T. H. Nam[2], Tran Q. Vinh[2], Cristina Martínez[3*], Vasile I. Parvulescu[4*]

[1*] *School of Chemical Engineering, Hanoi University of Science and Technology, 1 Dai Co Viet, Hanoi, Vietnam*, E-mail: *huyen.phamthanh@hust.edu.vn*

[2]Institute of Chemistry, Vietnam Academy of Science and Technology, Vietnam

[3] Instituto de Tecnología Química, Universitat Politècnica de València – Consejo Superior de Investigaciones Científicas, Spain

[4] Department of Organic Chemistry, Biochemistry and Catalysis, University of Bucharest, Romania, Email: *vasile.parvulescu@chimie.unibuc.ro*

Abstract

Al-SBA-15 and ZSM-5/SBA-15 (ZSC) composite were synthesized following hydrothermal procedures in the presence of triblock copolymer Poly(ethylene glycol)-poly(propylene glycol)-poly(ethylene glycol) (Pluronic P123) and a mixture of tetrapropylammonium bromide (TPABr)/Pluronic P123 templates, respectively. Pt(0.5wt.%)/Al-SBA-15 and ZSC bifunctional catalysts were then prepared by a wet impregnation methodology and investigated in the hydrocracking/hydroisomerization of *n*-decane. Pt/ZSC, containing a trimodal porous texture and high Brønsted acidity, exhibited hydrocracking activity while Pt/Al-SBA-15, showing merely Lewis acidity, was active for hydroisomerization. At 300^{o}C the conversion of *n*-decane on Pt/ZSC reached 98% and cracking selectivity was about 99%. Both catalysts were exhaustively characterized.

Keywords: ZSM-5/SBA-15 composite, Pt(0.5wt.%)/Al-SBA-15 and Pt(0.5wt.%)/ZSM-5/SBA-15 catalysts, hydrocracking and hydroisomerization of *n*-decane

1. Introduction

Despite the increasing importance of energy and fuel sources alternative to oil, there is a large dependency of both sectors on this fossil source, and, therefore, nowadays there is a constant need for the conventional refinery process optimization and the efficiency increase. However, the oil reserves are being depleted and, therefore, the refineries which are using light crude oils (such as Binh Son refinery, Vietnam) will have to seek new feedstocks of heavy crude oil in the near fulture. Heavy crude oil are more difficult to convert, due to their higher C/H molar ratio and the presence of heteroatoms such as sulfur, nitrogen or heavy metals (Ni, V), which may end up in the products obtained, decreasing their quality, or on the catalyst, decreasing its activity. The two main conversion processes are fluid catalytic cracking (FCC) and hydrocracking [1]. The latter presents a significant advantage over FCC, as it combines the cracking reactions with removal of the heteroatoms, especially sulfur, from the hydrocracked product streams.

The catalysts for hydrocracking/hydroisomerization of n-alkanes are bifunctional and contain acid and metal sites which have to be equilibrated and in close proximity in order to enhance the C-C bond breaking and hydrogenation of the unsaturated produced during the cracking [2-5]. The reaction mechanism and the influence of hydrogenation activity and molecular weight of the n-alkane on the final product distribution was already described in the early 1960's by Coonradt and Garwood *[Coonradt, H.L. and Garwood, W.E., Ind. Eng. Chem. Process Res. Dev. 3(1) (1964) 38-45]*, and later reviewed by others

[Martens, J.A. and Jacobs, P.A., Zeolites 6 (1986) 334-348;] ADD MORE REFERENCES AND SOME COMMENTS.

The acidity of the catalyst has a major influence on both the hydroisomerization and hydrocracking yields. The acid site density and acid strength distribution are both important and the proper balance of these variables is critical in determining the reactivity and selectivity of the bifunctional catalysts [6, 7]. ADD MORE REFERENCES AND SOME COMMENTS

Besides the metal site and the acidity, other characteristics of the supports, such as the pore size distribution or surface area, represent important elements controlling the bifunctional catalyst performances [8] ADD MORE REFERENCES AND SOME COMMENTS. To date, many supports with various pore sizes and different acidity, such as microporous [9 - 14], mesoporous [2, 15] or mixtures of micro-mesoporous [6, 8] materials have already been reported. Among these, On and Kaliaguine [16] reported the successful synthesis of materials presenting semi-crystalline zeolitic mesoporous walls. This kind of multimodal porous materials combines some advantages of micro- and mesoporous materials such as hydrothermal stability, high acidity, crystalline structure with the presence of well-defined micropores and ordered mesoporous structure, and a high surface area [17].

Based on this state of the art, the aim of this study was to investigate the behavior of a SBA-15 modified by Al and a composite of SBA-15 with ZSM-5 (noted as ZSC) taking as reaction model the hydrocracking of *n*-decane. Using such supports it was investigated both the effect of acidity and the support pore size.

2. Experimental

Catalysts synthesis

A ZSM-5/SBA-15 composite (ZSC) was synthesized according to an already reported procedure by Nam *et al* [17]. The samples were synthesized via three steps. In the step 1, seed 1 was synthesized from a homogeneous gel solution of 12.84 g Ludox AS-40, 0.71g $Al_2(SO_4)_3.18H_2O$ dissolved in 55 mL H_2SO_4 0.45 M and 1 g tetrapropylammonium bromide (TPABr) dissolved in 4 mL H_2O. The resulting gel was aged for 24 h and crystallized at 170°C for 8 h while stirring. Before the composite material formation step, seed 1 was added with 3.77 g Ludox AS-40 precursor in the step 2. The mixture was hydrothermally treated at 100ºC for 6 h while stirring to form seed 2. The synthesis of the mesoporous material, in step 3, was performed by adding the mixture obtained from the step 2 to a solution of 3 g Pluronic (P123) dissolved in 80 mL H_2SO_4 1.52 M . The resulting mixture was hydrothermally treated at 90°C for 24 h. The solid product was filtered and washed using deionised water to pH = 7, dried at 100°C, and calcined at 550°C for 5 h to remove the TPABr and P123 templates.

Al-SBA-15 was synthesized from 3.5 grams of P123 dissolved in 100 mL of 1.5 M HCl under vigorous stirring. After that, 0.6 g of aluminum sulfate were added and the solution was stirred for another hour. Then, 8.5 g of TEOS were gradually dropped and the solution was maintained at room temperature for 15 h, and at 40 ˚C for another 24 h. The obtained suspension was crystallized at 90 ˚C for 48 h in an autoclave. Then the solid product was filtered, washed with double distilled water, dried and calcined at 550 ˚C for 6 h (heating rate of 1 ˚C min^{-1}). SBA-15 was prepared following the same procedure as for Al-SBA-15 but without adding aluminum sulfate.

The deposition of Pt (0.5 wt.%) on these supports was carried out by a wet impregnation methodology as described in a previous paper [18].

Catalysts characterization

The N_2 adsorption–desorption isotherms were recorded at -196 °C using a Micromeritics ASAP2020 automated instrument. Prior to analysis, the catalysts containing Pt were pre-treated in a H_2 flow (300 mL min^{-1}) at 400 °C for 2h with a heating rate of 0.5 °C min^{-1}, then cooled in H_2, exposed to argon (30 mL min^{-1}) for 30 min, and then degassed for 15 h at 150 °C and 1.3×10^{-9} atm. Surface areas were estimated according to both the Langmuir and BET models, and the pore sizes were calculated using the micropore and BJH methods.

Powder X-ray diffraction patterns were recorded with a Phillips PW 1830 diffractometer using the CuKα radiation. Small and Wide angle XRD patterns were collected in steps of 0.02º (2θ) over the angular ranges (2θ) of 0.5–10º (SXRD) or 5–45º (WXRD) for 25 s per step.

The Pyridine-(Py) FTIR spectra were recorded with a IMPACT-410 (Germany) Infrared Spectrophotometer, with a resolution of 4 cm^{-1}. Prior to the adsorption the base, the powder samples were calcined at 450 ºC for 2 h under a flow of air (30 mL min^{-1}). Self-supporting wafers obtained by compression (about 12 mg cm^{-2}) were outgassed in the IR cell at 400ºC at a residual pressure of 1 atm. After the adsorption of Py, the samples were purged for 2 h with He (30 mL min^{-1}) at RT to remove the weakly sorbed species, and then heated at 150 ºC.

Transmission electron microscopy (TEM) analyses were performed with a JEOL JEM-1010 microscope at an accelerating voltage of 100 kV. Samples were prepared by powder dispersion in ethanol and subsequent deposition on a gold grid with carbon support.

Catalytic activity test

All the experiments were carried out in a fixed bed stainless steel reactor, using 0.3 g catalyst with particle size of 0.2-0.4 mm. The catalyst was *in-situ* pre-reduced in hydrogen (300 mL min^{-1}) at 400ºC for 2h. *n*-decane (1.56 g h^{-1}) was fed by means of a high pressure piston type pump. The reaction conditions corresponded to a H_2/substrate molar ratio of 9/1 or 18/1, pressure of 40 bars, temperatures in the range of 250 – 350ºC, and WHSV of 5.1 h^{-1}. The analysis of the gas and liquid products was carried out with a GC Varian STAR 3400 equipped with TCD and FID detectors using a FACTOR FOUR VF-1 MS column.

III. Results and discussion

Textural characterization

Figure 1 and Table 1 present the textural characteristics of the investigated catalysts.

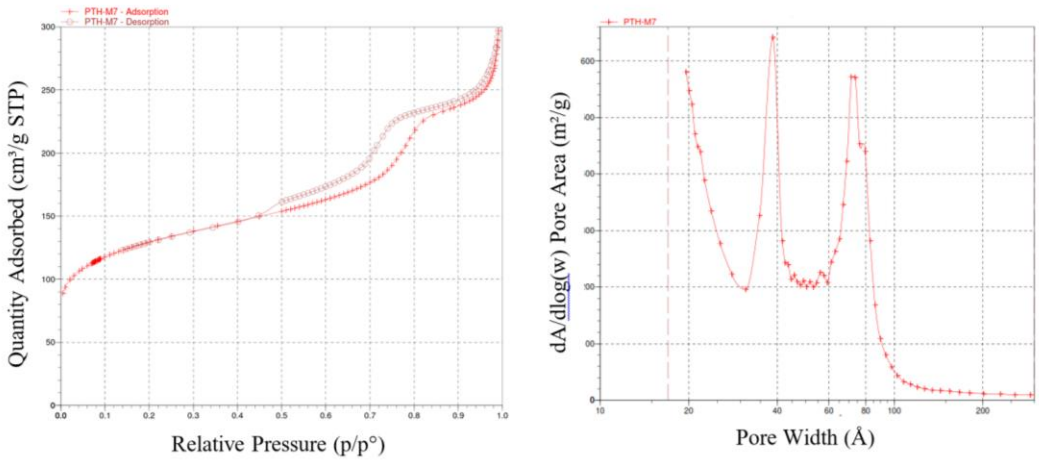

Figure 1. N_2 Isotherms and mesopore size distribution of Pt/ZSC

As expected, both BET and micropore surface areas of Pt/ZSC and Pt/Al-SBA-15 were smaller than those of the parent supports. In addition, for Pt/Al-SBA-15 the pore size distribution changed to bimodal with mesopores of 39 and 62 Å [18]. For the ZSC support, the micropore surface area was nearly half of the BET surface. However, after the deposition of Pt, the diminution of the surface occurred merely in the mesopore range, and micropore surface increases (see Table 1). It would be possible that the wet impregnation for Pt incorporation (performed in an aqueous solution) could wash out some amourphous debris, cleaning in this way part of the micropores, or part of mesopores being transformed in micropores. As can be seen in Table 1, there is a good agreement of the target and real Pt content in both catalysts.

Table 1. Textural characteristics of Pt/ZSC and Pt/Al-SBA-15 catalysts

Sample	BET surface area $m^2\ g^{-1}$	*t*-plot micropore surface area $m^2\ g^{-1}$	Pore volume $cm^3\ g^{-1}$	Pore size Å	Si/Al (ICP result)	Pt (ICP result) wt.%
ZSC	541	254	0.51	40, 75	51.01	-
Pt/ZSC	437	280	0.45	39, 72	50.77	0.49
Al-SBA-15	697	289	1.04	90	28.96	-
Pt-Al-SBA-15	684	255	0.79	39, 62	27.63	0.51

XRD characterization

The SXRD and WXRD patterns of the supports and catalysts are shown in Figure 2. The presence of platinum was not detected in the XRD patterns of both catalysts that can be

explained by the existence of highly dispersed small metal particles [18]. These diffractograms also confirmed the well-defined pattern of ZSM-5 in both the Pt free and Pt containing samples. For ZSC, the addition of Pt led to a decrease of the pore size (as also seen from the textural characterization).

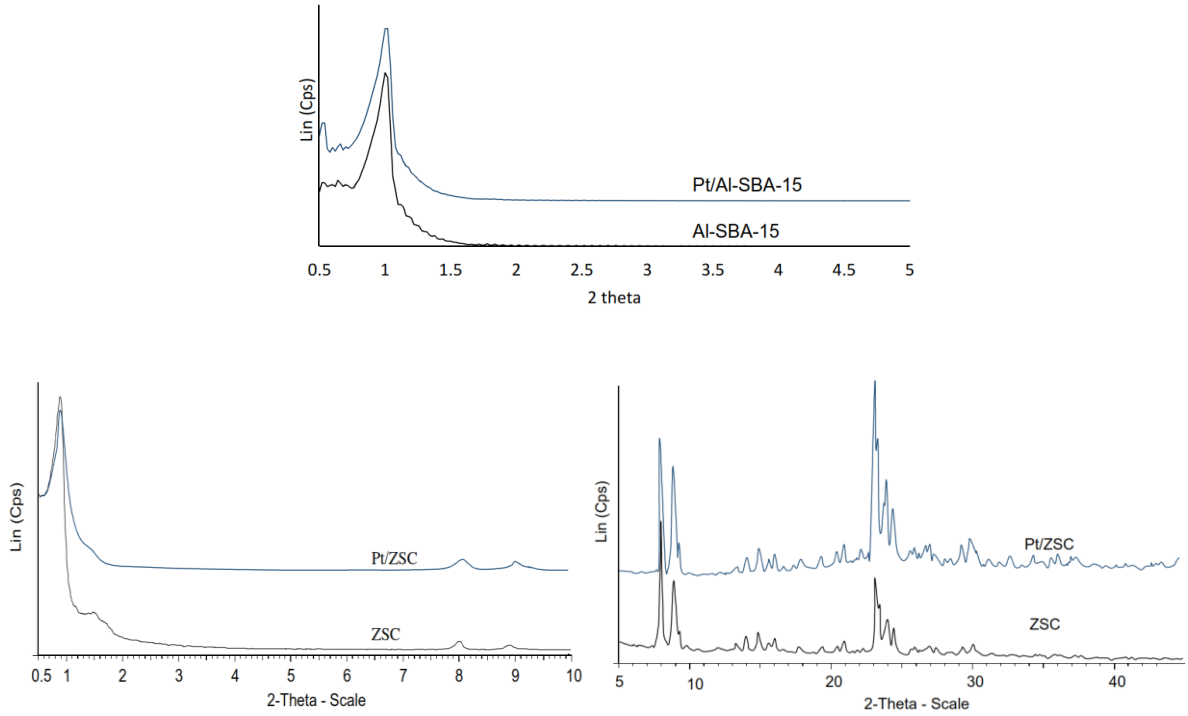

Figure 2. XRD patterns of Al-SBA-15, ZSC (small angle and wide angle) and supported Pt catalysts

TEM measurements

TEM pictures of the investigated catalysts are presented in Figure 3. They show a better dispersion of platinum on Al-SBA-15 than ZSM-5/SBA-15 composite support (Figure 3) that may also explain the differences in the measured surface areas (See Table 1). The ordered mesoporous structure of SBA-15 is not very clear in the TEM of ZSC that might

be explained by the presence of embedded small ZSM-5 crystallites in the amorphous walls of SBA-15. Such a behavior results in a semicrystalline wall structure, so that the walls are less defined than in the Al-SBA-15.

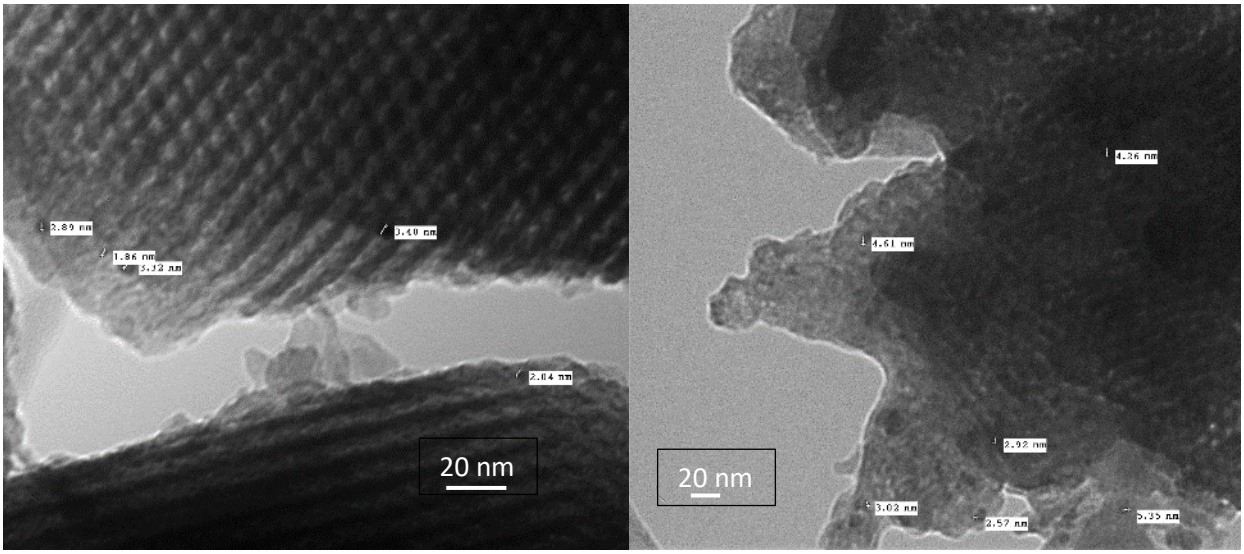

Figure 3. TEM pictures of Pt/Al-SBA-15 (left) and Pt/ZSC (right)

The Py-FTIR spectra of Pt/ZSC catalysts compared to those of Pt/SBA-15 and Pt/Al-SBA-15 are shown in Figure 4.

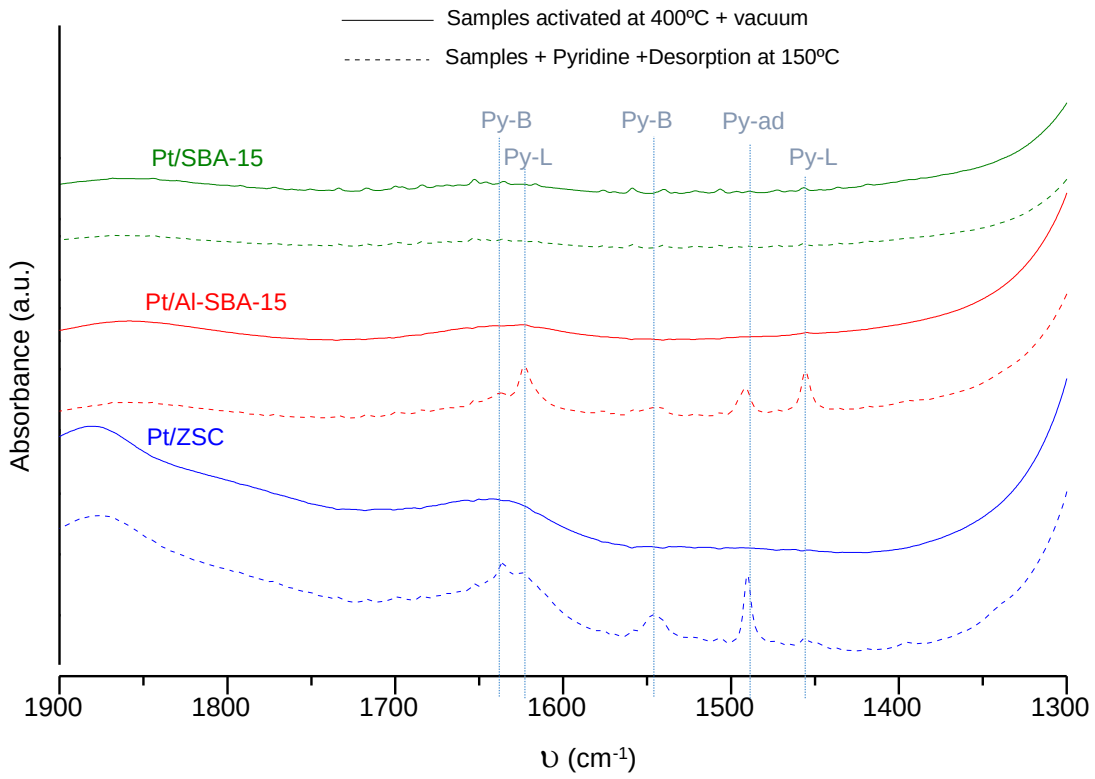

Figure 4. Py-FTIR spectra of Pt/ZSC catalysts compared to Pt/SBA-15 and Pt/Al-SBA-15

They indicate that Pt/SBA-15 exhibits no acidity (no pyridine adsorption has been detected on this catalyst). For the Pt/ZSC and Pt/Al-SBA-15 catalysts the Py-FTIR spectra evidence the presence of the acidity. The bands at 1622 and 1453 cm^{-1} account to the vibration modes of pyridine adsorbed on Lewis site (Py-L) [2, 18], and the absorption bands at 1636 and 1540 cm^{-1} were assigned to the basic probe interacting with Brønsted acid sites (Py-B). Pyridine adsorbed (Py-ad) on either Lewis or Brønsted sites can be seen at 1490 cm^{-1}. Although not quantified, these spectra suggest that the population of the Lewis acid sites on Pt/Al-SBA-15 is much higher than that on Pt/ZSC catalyst, whereas the Brønsted acid site density in Pt/ZSC is larger than that on Pt/Al-SBA-15. The higher Lewis acidity and lower Brønsted acidity of Pt/Al-SBA-15 as compared to Pt/ZSC might be due to the lower Si/Al ratio of Pt/Al-SBA-15 (27.6) compared to that of Pt/ZSC (50.8) that corresponds to a larger population of Lewis sites on Pt/Al-SBA-15. On other hands, it is more due to the amorphous nature of this material and its lower stability. It has been described that during Pt incorporation in aqueous media the Brønsted acid sites in Al-SBA-15 are converted into strong Lewis sites [19]. These results also confirm the fact that the modification of SBA-15 by Al and ZSM-5 increased the acidity of the catalysts.

Catalytic behavior

The first aspect to be noted is that Pt/SBA-15 exhibited no hydrocracking activity that is in concordance to the absence of the acidity (results not shown).

Figure 5 shows the influence of the reaction temperature and support on the hydrocraking of *n*-decane onto Pt/ZSC and Pt/Al-SBA-15 catalysts. The chromatographic analysis

including the distribution of the reaction products for *n*-decane hydrocracking on Pt/ZSC and Pt/Al-SBA-15 catalysts is compiled in the Tables 2 and 3, respectively.

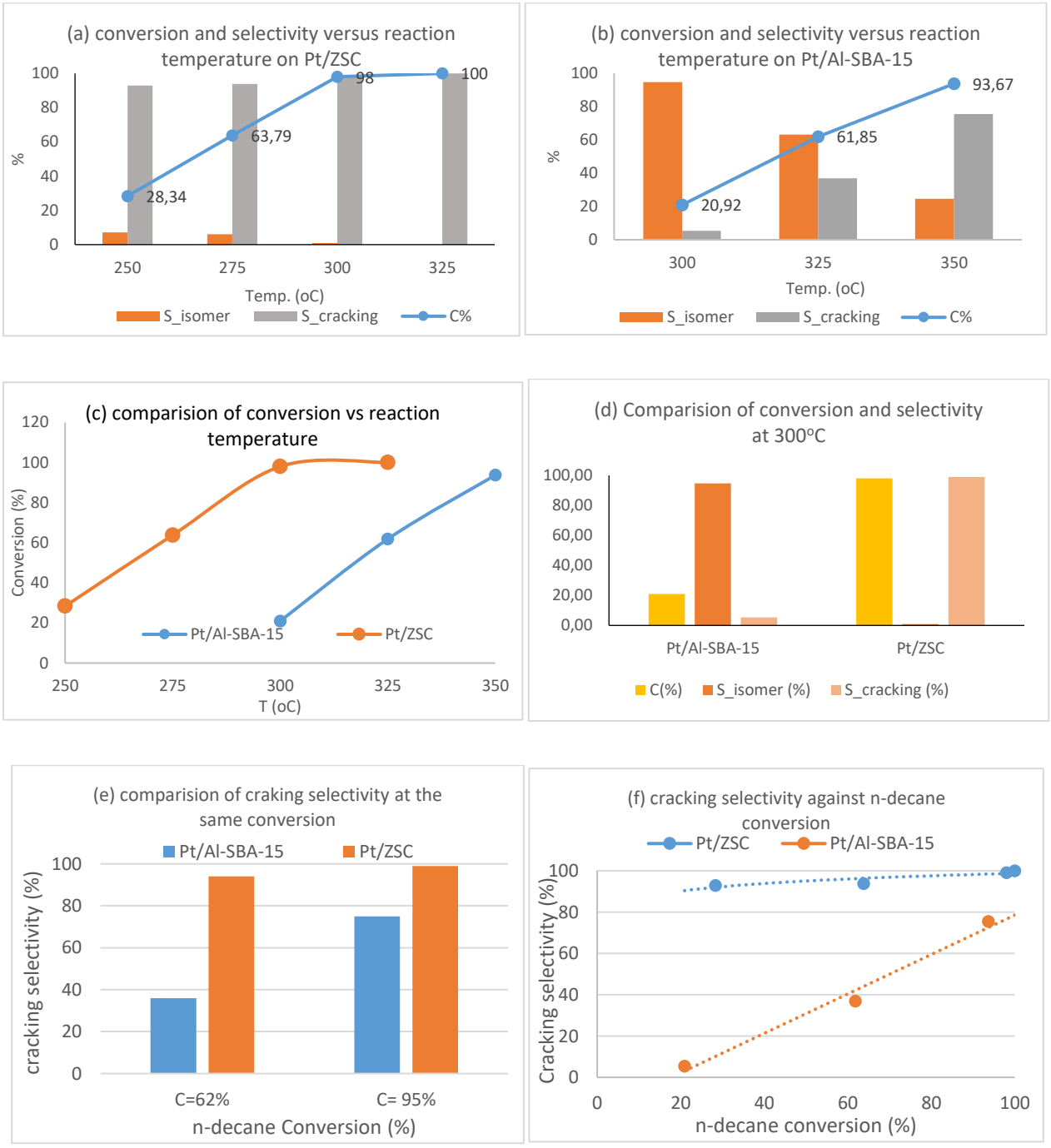

Fig.5. Influence of temperature and supports for the *n*-decane hydrocracking/hydroisomerization: a, b) conversion and selectivity versus reaction temperature on Pt/ZSC and Pt/Al-SBA-15; c) comparision of conversion vs reaction temperature on Pt/ZSC and Pt/Al-SBA-15; d) comparision of conversion and selectivity at

300ºC; e) comparision of craking selectivity at the same conversion; f) cracking selectivity against n-decane conversion. (WHSV = 5.2h^{-1}, H_2/n-C10=9, P=40bar)

Pt/ZSC showed high catalytic activity for the hydrocracking. At 300ºC, the conversion of *n*-decane reached 98% with a cracking selectivity of about 99% on Pt/ZSC, whereas the conversion of *n*-decane was only 20.92% and cracking selectivity was only 5.37% on Pt/Al-SBA-15.

For Pt/Al-SBA-15 conversions of around ~93% were obtained at higher temperature (350ºC), and with a much smaller cracking selectivity (~75%). Compared to Al-SBA-15, the ZSC composite preserved a superior selectivity to cracking independently of the conversion at which they were evaluated. In both cases, hydrocracking is dominating at high conversions [20].

The analysis of the results presented in Tables 2 and 3 also shows that while Pt/ZSC (which contains both miro- and mesopores) favored the hydrocracking reaction, Pt-Al-SBA-15 stimulated the isomerization one. Thus, Pt-Al-SBA-15 led to the highest isomerization selectivity (94.6% at 300ºC) for a *n*-decane conversion of 20.9%

Isomerization and hydrocracking of an n-alkane occur on bi-functional catalysts following the classical mechanism involving the formation of an alkylcarbenium ion. Accordingly, the alkane is firstly dehydrogenated onto the metal site to alkene, which is then protonated by a Brønsted acid site to form an alkylcarbenium ion [7, 12]. Pt/ZSC presented a multimodal porous structure and higher Brønsted acidity. These characteristics may explain the hydrocracking capability of this catalyst comparing to hydroisomerization. Figure 6 depicts the reaction pathway on the investigated catalysts.

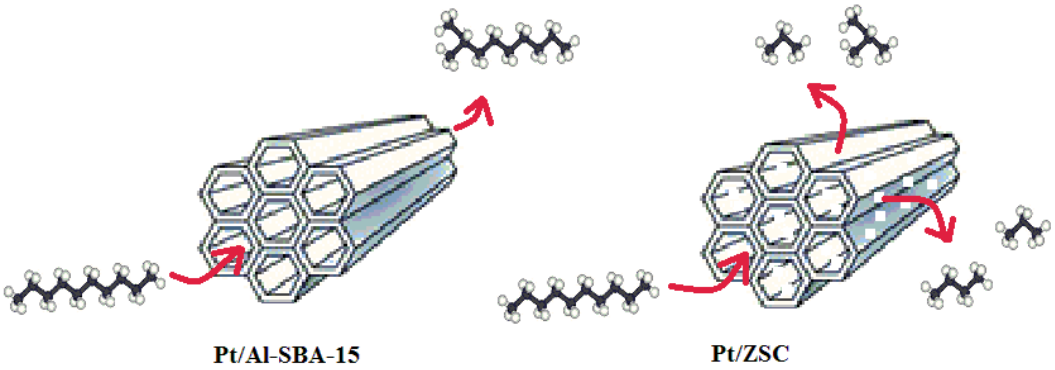

Fig.6. Reaction pathway for the hydroisomerization/hydrocracking of *n*-decane onto the Pt/Al-SBA-15 and Pt/ZSC catalysts**.**

Table 2. Gas product analysis for n-decane hydrocracking on Pt/ZSC catalyst (WHSV = $5.2h^{-1}$, H_2/n-C_{10}=9, P=40bar)

Temp. (°C)	250	275	300	325
n-decane conversion (%)	28.34	63.79	98.00	100.00
Cracking selectivity (%)	92.90	93.77	99.05	100.00
C1	0.078	0	0	0.07
C2	0	0.07	0.14	0.43
C3	17.7	19.4	19.4	23.2
i-C4	10.6	12.9	14.6	17.2
n-C4	14.4	15.1	14.5	16.1
i-c5	6.2	7.9	9.3	11.2
n-c5	14.5	14.3	13.7	12.1
$C5^{=}$	4.32	0.002	0.001	0.001
C6+	31.83	29.857	27.89	19.37
unknown	0.372	0.471	0.469	0.329

total	100	100	100	100

Table 3. Gas product analysis of the n-decane hydrocracking on Pt/Al-SBA-15 catalyst (WHSV = 5.2h^{-1}, H_2/n-C_{10}=9, P=40bar)

Temp. (^oC)	300	325	350
n-decane conversion (%)	20.92	61.85	93.67
Cracking selectivity (%)	5.37	36.91	75.46
C1	0	0	0
C2	0	0	0
C3	19.20	18.90	18.60
i-C4	9.40	9.36	9.20
n-C4	10.60	11.80	12.50
i-c5	7.90	7.64	7.30
n-c5	9.40	9.69	10.10
$C5^=$	0.01	0.01	0.01
C6+	43.28	42.37	42.09
unknown	0.21	0.23	0.20
total	100	100	100

Very small amounts of methane and ethane were also found in the hydrocracking gas phase products on Pt/ZSC catalyst. According to reports of Elangovan and Hartmann, the presence of such molecules might be an indication of an ionic mechanism of cleavage under the hydrocracking conditions [6]. At low temperatures, very small amounts of $C5^=$ were also detected and could be explained by an inefficient hydrogenation capacity at this temperature.

Figure 7 depicts the influence of the H_2/feed molar ratio on the catalytic activity of Pt/ZSC for *n*-decane hydrocracking and the evolution of the conversion in time. The collected results demonstrated that an increase of this ratio led to the decrease of the conversion because of the lower partial pressure of n-decane. More important is the evolution of the conversion in time, where the results showed that on Pt/ZSC no fast deactivation occurred. Such a behavior may indeed recommend this support for the production of catalysts for hydrocracking.

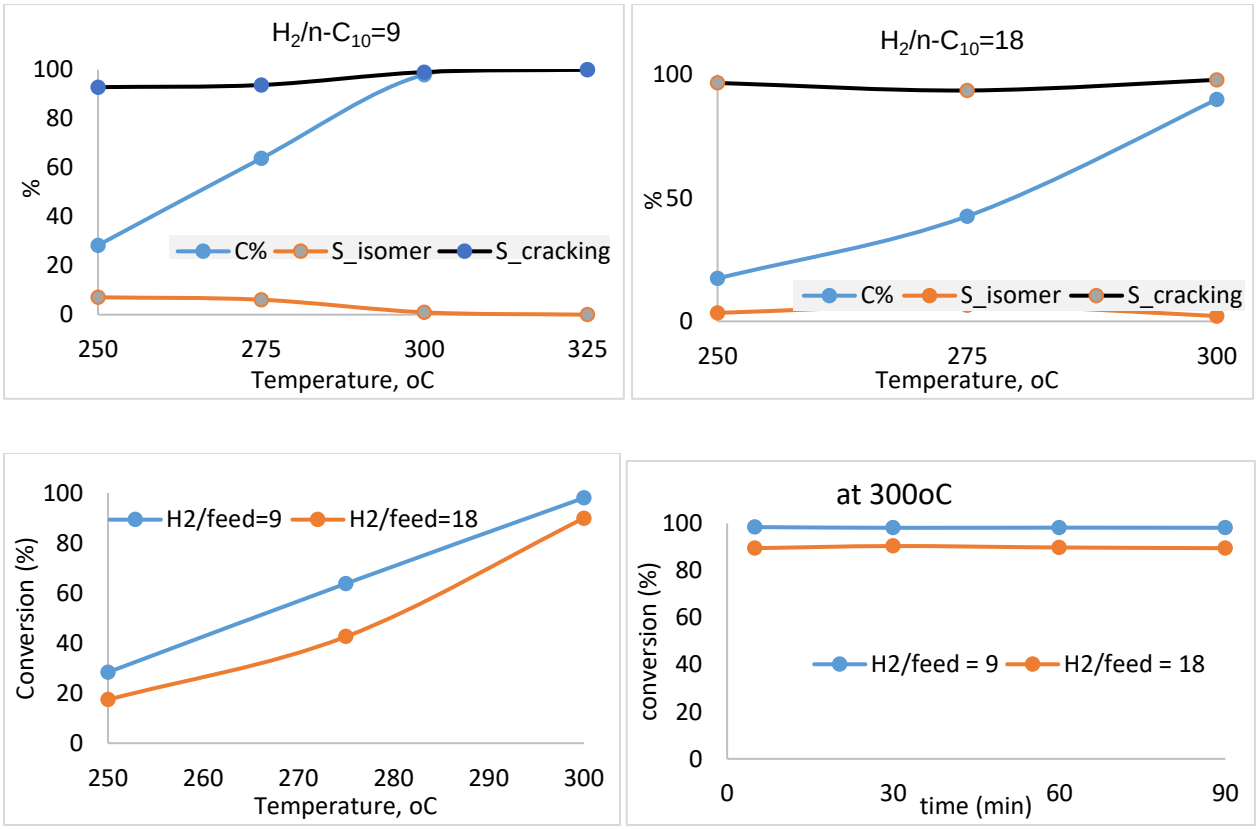

Fig.7. Influence of temperature and time for *n*-decane hydrocracking of Pt/ZSC at different H_2/*n*-decane molar ratios (WHSV = 5.2h^{-1}, P=40bar)

Conclusions

The composite ZSC support prepared in this study can be synthesized following a simple and reproducible procedure. Its characterization demonstrated a trimodal pore size

distribution in which the walls formed from microporous ZSM-5 generated a bimodal mesoporous texture. Py-FTIR measurements showed that this material exhibits acidic properties where the Brønsted acid site density is larger than that in Pt/Al-SBA-15. For the Al-SBA-15 dominated the Lewis acidity. The deposition of Pt on this support occurred in a less uniform shape as for Al-SBA-15.

The evaluation of the catalytic activity in the hydrocracking of *n*-decane demonstrated that both the conversion and the selectivity depended on the acidity and the pore size of the catalyst. A higher Brønsted acidity coupled to the existence of the zeolitic mesopore walls afforded good catalyst performances for hydrocracking. Oppositely, Pt/Al-SBA-15 was found as a suitable catalyst for hydroisomerization. The homogeneity of Pt particles on the support appeared as being less important in this stage. Such a behavior may indeed recommend the ZSC support as suitable for the synthesis of catalysts for hydrocracking.

Acknowledgement: This research is funded by Vietnam National Foundation for Science and Technology Development (NAFOSTED) under grant number 104.05-2014.21

References

1. W. Vermeiren, J.-P. Gilson, Top. Catal. 52 (2009)1131–1161.
2. A. Corma, A. Martinez, S. Pergher, S. Peratello, C. Perego, G. Bellusi, Appl. Catal. A 152 (1997) 107-125.
3. V. Calemma, S. Peratello, C. Perego, Appl. Catal. A 190 (2000) 207-218.
4. R. Sahu, B. J. Song, J.S. Im, Y-P. Jeon, C.W. Lee, J. Ind. Eng. Chem. 27 (2015) 12–24.
5. C. Martínez, A.Corma, Coord. Chem. Rev. 255 (2011) 1558–1580.
6. S.P. Elangovan, M. Hartmann, J. Catal. 217 (2003) 388–395.
7. H. Deldari, Appl. Catal. A: General 293 (2005) 1–10.

8. R. Kenmogne, A. Finiels, C. Cammarano, V. Hulea, F. Fajula, J. Catal. 329 (2015) 348–354.
9. A. Martínez, M.A. Arribas, M. Derewinski, A. Burkat-Dulak, Appl. Catal. A: General 379 (2010) 188–197.
10. S. Fernandes, M. Andrade, C. O. Ania, A. Martins, J. Pires, A. P. Carvalho, Micropor. Mesopor. Mater. 163 (2012) 21–28.
11. M. Guisnet, Catal. Today 218–219 (2013) 123–134.
12. E. Verheyen, C. Jo, M. Kurttepeli, G. Vanbutsele, E. Gobechiya, T. I. Korányi, S. Bals, G. V. Tendeloo, R. Ryoo, C. E.A. Kirschhock, J. A. Martens, J. Catal. 300 (2013) 70–80.
13. J. A. Martens, D.Verboekend, K. Thomas, G.Vanbutsele, J. P.-Ramírez, J.-P. Gilson, Catal. Today 218–219 (2013) 135–142.
14. N. Kasian, E. Verheyen, G. Vanbutsele, K. Houthoofd, T. I. Koranyi, J. A. Martens, C. E.A. Kirschhock, Micropor. Mesopor. Mater. 166 (2013) 153–160.
15. B.C. Gagea, Y. Lorgouilloux, Y. Altintas, P.A. Jacobs, J.A. Martens, J. Catal. 265 (2009) 99–108.
16. D. T. On, S. Kaliaguine, Angew. Chem. 113 (2001) 3348-3351.
17. L.T.H. Nam, T.Q Vinh, N.D Hoa, M. Hunger, Int. J. Nanotechnol., 12 (2015) 466-474.
18. P.T. Huyen, M. Krivec, M. Kočevar, I. C. Bucur, C. Rizescu, V. I. Parvulescu, ChemCatChem, 2016, 8, 1–12.
19. S. Handjani, S. Dzwigaj, J. Blanchard, E. Marceau, J-.M. Krafft, M. Che, Top. Catal. 52 (2009) 334-343.
20. Y. Rezgui, M. Guemini, Appl. Catal. A: General 282 (2005) 45–53.